Title

Physical Modeling of Coupled Thermohydraulic Behavior of Compacted MX80 Bentonite during Heating

Journal

Geotechnical Testing Journal, 45(6)

ISSN

0149-6115

Authors

Lu, Yu

McCartney, John Scott

Publication Date

2022-11-01

DOI

10.1520/gtj20220054

Peer reviewed

Geotechnical Testing Journal

Physical Modeling of Coupled Thermo-hydraulic Behavior of Compacted MX80 Bentonite during Heating

Journal:	*Geotechnical Testing Journal*
Manuscript ID	GTJ-2022-0054.R2
Manuscript Type:	Technical Manuscript
Date Submitted by the Author:	n/a
Complete List of Authors:	Lu, Yu; University of California San Diego, Structural Engineering McCartney, John; University of California San Diego, Department of Structural Engineering
ASTM Committees and Subcommittees:	D18.04 Hydrologic Properties and Hydraulic Barriers < D18 Committee on Soil and Rock
Keywords:	Bentonite, Coupled heat transfer and water flow, Unsaturated soil, Physical modeling, SWRC, Central heating
Abstract:	This paper describes a tank-scale test setup and experimental methodology used to investigate coupled heat transfer and water flow processes during heating of compacted MX80 bentonite to high temperatures. Specifically, a temperature of 200 °C was maintained by a cylindrical heating element at the center of a compacted bentonite layer containing an array of temperature, dielectric, and relative humidity sensors. In addition to providing an evaluation of the spatio-temporal variations in temperature, relative humidity, degree of saturation, and global volume, the coupled thermo-hydraulic properties of the bentonite were assessed. A wetting front was initially observed to move away from the central heater, followed by a drying process until reaching thermo-hydraulic equilibrium. The soil-water retention curve (SWRC) of the bentonite followed a wetting scanning path before following the primary drying path exhibiting a shift in water retention with elevated temperature. Results from the tank-scale test can be used for validation of numerical simulations of drying processes in the engineered barrier system of a high-level radioactive waste geological disposal repository and confirm that a temperature-dependent hysteretic SWRC with scanning paths is required to accurately capture the bentonite response.

Physical Modeling of Coupled Thermo-hydraulic Behavior of Compacted MX80 Bentonite during Heating

Yu Lu, Ph.D.

Postdoctoral Researcher, Dept. of Structural Engineering, Univ. of California San Diego, 9500 Gilman Dr., La Jolla, CA 92093-0085; yul204@eng.ucsd.edu

John S. McCartney, Ph.D., P.E., F.ASCE (corresponding author)

Professor and Chair, Dept. of Structural Engineering, Univ. of California San Diego, 9500 Gilman Dr., La Jolla, CA 92093-0085; mccartney@ucsd.edu

ABSTRACT: This paper describes a tank-scale test setup and experimental methodology used to investigate coupled heat transfer and water flow processes during heating of compacted MX80 bentonite to high temperatures. Specifically, a temperature of 200 °C was maintained by a cylindrical heating element at the center of a compacted bentonite layer containing an array of temperature, dielectric, and relative humidity sensors. In addition to providing an evaluation of the spatio-temporal variations in temperature, relative humidity, degree of saturation, and global volume, the coupled thermo-hydraulic properties of the bentonite were assessed. A wetting front was initially observed to move away from the central heater, followed by a drying process until reaching thermo-hydraulic equilibrium. The soil-water retention curve (SWRC) of the bentonite followed a wetting scanning path before following the primary drying path exhibiting a shift in water retention with elevated temperature. Results from the tank-scale test can be used for validation of numerical simulations of drying processes in the engineered barrier system of a high-level radioactive waste geological disposal repository and confirm that a temperature-dependent hysteretic SWRC with scanning paths is required to accurately capture the bentonite response.

KEYWORDS: Bentonite, Coupled heat transfer and water flow, Unsaturated soil, Physical modeling, SWRC, Central heating~~Heat transfer~~

INTRODUCTION

The permanent disposal of high-level radioactive waste to protect humans and environment in the long term is one of the major technical hurdles that must be addressed for nuclear energy to remain a viable energy source (e.g., Birkholzer et al. 2012). A disposal option that has been under investigation for more than 40 years is the storage of waste canisters in deep geological repositories (e.g., Pusch 1979~~, 1992~~; Börgesson et al. 1994). A key component of geological repositories is the compacted bentonite placed as a buffer between the waste canister and the surrounding host rock (e.g., Lloret et al. 2003; Schanz and Al-Badran 2014). Observations from long-term field studies on bentonite buffers indicate that distributions of temperature, degree of saturation, and dry density of the compacted bentonite will vary during the operation of the repository due to the combined effects of heat released by the waste canister and hydration from groundwater in the host rock, which will inevitably affect the long-term buffer performance (e.g., Börgesson et al. 2001; Villar 2020). An example of the coupled heat transfer and water flow processes in a bentonite buffer surrounding a waste container is shown in Figure 1. Simulations of the thermo-hydro-mechanical response of bentonite buffers must capture these coupled processes to accurately predict their long-term behavior.

A key challenge is that the hysteretic thermo-hydraulic properties of compacted bentonite are still not well understood. This is particularly the case when waste canister temperatures approach values as high as 200 °C (e.g., Zheng et al. 2015; GTS 2022). These properties, which are highly coupled, include those governing water retention, water transport in liquid and vapor forms, heat transfer, and volume change due to changes in temperature or water content. Although it is possible to perform element-scale tests to measure parameters like the soil-water retention curve (SWRC), hydraulic

conductivity function, thermal conductivity function, volumetric heat capacity function, or thermo-elastic volume change response, an important way to understand the coupled thermo-hydraulic behavior of a bentonite buffer is to perform tank-scale tests where relevant variables like temperature, relative humidity, volumetric water content, and volume are carefully monitored over time to evaluate the transient thermo-hydro-mechanical paths at different distances from the heater. An improved understanding of these couplings is necessary as many simulations of heat transfer and water flow in bentonite buffers used the thermo-hydraulic parameters measured at room temperature without consideration of the effects of hydraulic hysteresis (e.g., Sánchez et al. 2005; Zheng et al. 2017). Accordingly, the main objective of this study is to evaluate the spatial distribution of temperature and relative humidity/volumetric water content of a bentonite layer subjected to central heating conditions. For this purpose, a heating element was installed within a layer of bentonite compacted within a cylindrical tank, and sensors placed during compaction were used to track the transient thermo-hydraulic response of the bentonite layer during a 3.5 month-long heating process.

BACKGROUND

Although most researchers assume that a compacted bentonite buffer will eventually become fully saturated due to hydration from water in the surrounding host rock, the compacted bentonite in the repository is expected to be in unsaturated conditions for times on the order of decades, especially for the bentonite closest to the waste canister. The transient coupled heat transfer and water flow process will determine the long-term density distribution in the bentonite buffer and ensure the security of the waste container in the short term. The heat transfer in unsaturated soil and the movement of water in soil caused by thermal and hydraulic gradients has been studied experimentally extensively (e.g., Bouyoucos 1915; Gurr et al. 1952; Gens et al.

1998; Moradi et al. 2015; Başer et al. 2018; Lu et al. 2020). Some general observations have been summarized by Başer et al. (2018) as heat transfer occurs in unsaturated soil by conduction, convection in both liquid and gas phases, and latent heat transfer associated with water phase change, while conduction is assumed to be the primary mode. Water movement due to a temperature gradient is controlled by both vaporization and condensation processes as well as the development of suction gradients caused by changes in water properties with temperature and drying effects. The magnitude of thermally induced water flow depends on the initial degree of saturation, and the times required to reach steady-state distributions in the degree of saturation and temperature may be different depending on the thermal and hydraulic properties of a given soil, which may also be coupled. Many researchers have confirmed that the forms and properties of water, including the density of liquid water (e.g., Kell 1977~~; Jacinto et al. 2012~~), dynamic viscosity of liquid water (e.g., Kestin et al. 1978), the air-water surface tension (e.g., de Jonge et al. 1999~~; Bachmann 2002~~), relative humidity at equilibrium (e.g., Philip and de Vries 1957), saturated vapor concentration in the gas phase (e.g., Campbell 1985), vapor diffusion coefficient in the air (e.g., Campbell 1985), and the latent heat of water vaporization (e.g., Henderson-Sellers 1984), are dependent on temperature. However, previous studies on the impacts of these variables in bentonites mainly focused on the investigation of specific parameters in element-scale tests where boundary and size effects would inevitably influence the measured results (e.g., Saba et al. 2014a, 2014b; Tripathy et al. 2014).

Several full-scale tests have been carried out or started either in-suit or in the laboratory under the coupled thermo-hydro-mechanical conditions (e.g., ~~Alonso et al. 2005;~~ Gens et al. 2007; GTS 2022). For example, the Full-scale Engineered Barriers Experiment (FEBEX) test was commissioned at the Grimsel underground research

laboratory in Switzerland (Alonso et al. 2005). Similarly, a laboratory-based full-scale mock-up experiment was conducted as a forerunner of the FEBEX test under boundary control conditions (Martín and Barcala 2005). While valuable in providing actual repository construction effects and boundary conditions, they have high installation and operating costs. Alternatively, several small-scale column tests (which can be regarded as 1-D analysis) have been performed which also have precise control over the applied thermal and hydraulic gradients, efficient data monitoring, and a reasonable testing period (e.g., Cuevas et al. 1997; Yong et al. 1997; Börgesson et al. 2001; ~~Pintado et al. 2002; Villar et al. 2005;~~ Åkesson et al. 2009; Ye et al., 2009; Schanz et al. 2013; Saba et al. 2014b; Tripathy et al. 2015; Rawat et al. 2019, 2020, 2021). For instance, Rawat et al. (2021) developed a column-type experimental device for investigating the coupled thermo-hydro-mechanical behavior of expansive soils, with which temperature gradient can be applied at the opposite ends of the specimen to investigate the features (e.g., water flow, volumetric change, anisotropic swelling pressure) of temperature-driven processes in unsaturated compacted porous media.

An issue with the past in-situ and column studies is that the temperatures applied were generally below 100 °C. New repository conditions being explored involve waste canister temperatures up to 200 °C. For example, the recently started full-scale in-situ HotBENT experimtne involves a maximum heater temperature of 200 °C (GTS 2022). Zheng et al. (2015, 2017) conducted a coupled THMC simulation of a nuclear waste repository in a clay formation with bentonite backfilled EBS for 1000 years, with the temperature in the bentonite near the waste canister can reach about 200 °C. However, they used the thermo-hydraulic properties of bentonite measured at room temperature for simulations. Information on higher temperatures on buffers is desirable for repository optimization concerning design, space and costs (e.g., footprint, layout) and

to enable more options with respect to the required interim storage periods (GTS 2022). Meanwhile, the thermal gradient in previous work was typically applied on the opposite ends of the isometric column specimen (parallel to the compaction direction of the specimen), while the nonnegligible radial temperature gradient in the geological repository is from the canister (decay heat) in the center to the variable section buffer material surrounded and then the host rock. In which, the thermal conductivity is perpendicular to the compaction direction of bentonite blocks, while the anisotropy of thermal behavior has been confirmed in compacted bentonite (e.g., Lee et al. 2016; Lu et al. 2020). Thus, investigation of the spatial distributions of temperature and relative humidity/volumetric water content in large-scale bentonite layers under long-term high-temperature heating can better capture the coupled processes representative of the repository operating conditions, is still worth studying in more detail.

Meanwhile, numerical model investigation for coupled heat transfer and flow of water in liquid and vapor forms have been investigated for unsaturated porous media both in nondeformable conditions (e.g., Philip and de Vries 1957; Thomas and King 1991; ~~Smits et al. 2011;~~ Başer et al. 2018), and deformable conditions (e.g., Gawin et al. 1995; ~~Thomas et al 1996;~~ Thomas and He 1997). Most models for nondeformable unsaturated soils are based on the model of Philip and de Vries (1957), who proposed the liquid island theory to explain the observations by Gurr et al. (1952) that vapor diffusion occurred at a faster rate than that predicted by Fick's law. They provided a pore-scale explanation where local thermal gradients are assumed to be higher across microscopic air-filled pores than the global thermal gradient across soil element, and where water vapor diffusion is enhanced by evaporation and condensation from water held between soil particles by capillarity, effectively increasing the area available for vapor diffusion through the soil element. The approaches proposed on deformable

unsaturated soils typically extend previous model analyses of the coupled transport of heat, pore water, and pore air to take account of the deformation behaviors of unsaturated soil. For example, Thomas and He (1997) proposed a formulation based on a mechanistic phase interaction model (de Vries 1958) coupled to a state surface (Lloret and Alonso 1985), where the pore water pressure, pore air pressure, temperature, and displacement are treated as the primary unknowns. However, many simulations of heat transfer and water flow in bentonite buffers use thermo-hydraulic properties measured at room temperature (e.g., Sánchez et al. 2005; Zheng et al. 2017) as models to consider the effects of elevated temperatures are not yet available for expansive clays.

The SWRC of bentonite reflects all mechanisms of soil-water interactions and can be sensitive to temperature, density, constraint conditions, among other variables (e.g., Tuller et al. 1999; Romero et al. 2011). The pore water for the bentonite in the low suction range includes both the capillary water that exists in the pores between the aggregates and the adsorb water that exists in the pores within the aggregates, thus the water retention mechanism involves both capillary and adsorption effects. In the high suction range, the main water retention mechanism of bentonite is the adsorption effect, since the pore water mainly consists of adsorbed water existing in the pores of the aggregate. Increased temperature may lead to a decrease in water retention for the following reasons: (1) retention of water due to capillarity for suctions less than approximately 10 MPa is closely related to the liquid surface tension and contact angle, which will decrease with temperature, resulting in a decrease of capillary water content in bentonite (Villar 2004); (2) the increase in temperature causes the water in the aggregates to be released into the inter-particles pores to become free water thus reducing the water retention capacity of bentonite (e.g., Ma and Hueckel 1992); (3) the increase in temperature leads to a thermal expansion of closed air bubbles which will

displace capillary water, and lead to the capillary water decreases (e.g., Romero et al. 2003); (4) porosity redistribution and thermo-chemical interactions, which alter clay fabric and pore fluid, can be relevant (e.g., Romero et al. 2001), and (5) reductions in the maximum suction that the soil can sustain (e.g., Lu and Khorshidi 2015). An increase in adsorptive water retention may occur with temperature as the thickness of the diffuse double layer will increase with temperature (e.g., Revil and Lu 2013). Previous studies also found the influence of dry density on the water retention capacity depends on the suction range, while no consensus has been reached. For example, Jacinto et al. (2009) found for suctions above 30 MPa, the retention capacity of MX80 bentonite in terms of water content is higher as the dry density increases, whereas for suctions below this threshold value, the lower the dry density the higher the water content for a particular suction. Ye et al. (2015) found that the effect of initial dry density on water retention of GMZ01 bentonite is negligible for suctions greater than 10 MPa but can be significant for lower suctions. Meanwhile, a hysteretic behavior was witnessed between the wetting path and drying path on the SWRCs, which can be interpreted from the aspects of difference in pore size and its connection throat, change of pore structure, water-air interface contact angle, etc. (e.g., ~~Fredlund and Rahardjo 1993;~~ Rostami et al. 2013; Kim et al. 2018). Further, Dueck and Nillson (2010) observed hysteretic SWRCs in the high suction range during application of suctions using vapor equilibrium. Lu et al. (2015) further differentiated particle-surface hydration and crystalline or interlayer cation hydration to describe the hysteresis. It is important to note that most of the studies mentioned in this section focused on traditional "small-size cake-shaped" specimens (where suction inside is considered uniform) with suction control using the vapor equilibrium technique which means that there is a lack of investigation on the different transient thermo-hydraulic paths that a

compacted, unsaturated bentonite may undergo during heating, which will vary with the distance from the heater in the buffer.

MATERIALS

This study focuses on MX80 Bentonite from Wyoming, one of the most popular types of bentonites used internationally in bentonite buffer systems (e.g., Villar 2005; Wang et al. 2012). The MX80 bentonite used in this work was obtained from the American Colloid Company in granular form with a low initial gravimetric water content of approximately 9%. The geotechnical index properties of this bentonite are listed in Table 1. Bentonite is a naturally mined clay so its Atterberg limits are variable, but the liquid and plastic limits measured by the authors in this study are consistent those reported by Tripathy et al. (2014) and Bennett (2014). The grain size distribution curve of the bentonite in both granular forms using sieve testing and hydrated forms using hydrometer testing are presented in Figure 2(a). The relatively coarse grain size distribution of the granular bentonite MX80 bentonite indicates that a difference between the macropores between granules and the micropores within the granules will be present, which may affect the thermo-hydraulic properties. The SWRC of bentonite under room temperatures is shown in Figure 2(b) along with a best fit of the SWRC model proposed by Lu (2016) ~~with parameters in Table 4~~. The points on the SWRC were obtained for individual specimens of bentonite compacted to an initial dry density of 1.3 Mg/m^3 at a gravimetric water content of 12.55%, which were brought to different suction values using the vapor equilibrium technique (e.g., Tang et al. 2005). The specimens were tested under unconstrained conditions, so they were allowed to change in volume during hydration or drying from the initial conditions. Note that the shape of the SWRC is sensitive to the initial dry density (e.g., Villar 2005). Thus, the initial dry density of the specimen in Figure 2(b) selected the same value as adopted in the tank

test below. There are two reasons for choosing 1.3 Mg/m^3 as the initial dry density in this work. Firstly, 1.3 Mg/m^3 has been widely chosen as a target dry density in previous studies on bentonite (e.g., ~~Sawatsky and Oscarson 1991; Choi and Oscarson 1996;~~ ~~Bag 2011;~~ Villar 2005; ~~Hoffmann et al. 2007;~~ Cui 2017; Xu et al. 2017), which may help in interpretation of results. Secondly, it is challenging to reach high densities during manual compaction of granular MX80 via hand tamping into a tank with a large cross-sectional area. Manual compaction, as opposed to static compaction using a compression frame, is required to protect embedded sensors. The maximum dry density that can be achieved by manual compaction is approximately 1.3 Mg/m^3. Greater dry densities are achieved in the field by mixing bentonite pellets with granular bentonite, but the focus of this study is on granular bentonite.

EXPERIMENTAL INVESTIGATION

Experimental setup

For implementing the tank-scale heating test, an experimental setup was developed that consists of an insulated, cylindrical aluminum container, a heating system, and embedded sensors. A schematic of the setup is shown in Figure 3. The aluminum tank has an internal diameter of 554.5 mm, an external diameter of 587.5 mm, and a height of 477.8 mm. The aluminum has a density of 2.7 Mg/m^3, a thermal conductivity of 237 W/(m·K), and a specific heat capacity of 921 J/(kg·K). The upper surface of the bentonite is confined by a reinforced concrete cap (not fixed on the tank, and the displacement can be measured by LVDT) with a diameter of 540 mm, a height of 57.2 mm, and a mass of 48.78 kg. In this study, the cap was only used to maintain a stable soil surface during the heating test reported in this study but can also be used as part of an integrated loading system to apply axial loads to the soil layer to prevent volume changes during bentonite hydration. Mineral wool blanket insulation with a thickness

of approximately 100 mm was wrapped around the sides of the tank, below the tank, and above the concrete cap to help minimize heat losses from the setup.

The heating system consists of a Watlow Firerod 2127 cartridge heating element and a Watlow EZ-ZONE PM6 temperature controller. The cartridge heating element has 12.5 mm in diameter, 102 mm in height, and 1100 W in maximum power. A type K thermocouple is encapsulated in the middle of the heating element. The temperature controller with a calibration accuracy of ±1 °C was connected to the temperature controller to maintain a constant temperature at the center of the heater during testing.

The thermo-hydraulic response of the bentonite layer was monitored using four TE HTM2500LFL relative humidity sensors, five Meter Teros 12 dielectric sensors, and three Omega thermocouples (Type K). The relative humidity sensors contain a relative humidity and temperature module, with humidity calibrated within +/-2% at 55%RH, and temperature measurement through NTC 10 kOhms +/-1% direct output. The dielectric sensor together with the Em50 data logger provides measurement of volumetric water content with a resolution of 0.001 m^3/m^3 and accuracy of ±0.03 m^3/m^3, and temperature with a resolution of 0.1 °C and an accuracy of ±0.3 °C. The Type K thermocouples have a measurement range of 0 - 230 °C and were used to measure the soil temperatures on the top and side boundaries as well as the ambient room temperature. The vertical surface deformations during the heating process were measured using a Schaevitz 500HR Linear Variable Differential Transformer (LVDT) having a range of 25.4 mm and a sensitivity of 28 mV/V/mm. Two stable power supplies were used for the relative humidity sensors (5V DC) and LVDT (24V DC), respectively. A National Instruments data acquisition system, consisting of NI ethernet CompactDAQ chassis with C series universal analog input modules and computer with LabVIEW software, was used for data collection.

Soil layer preparation and sensor location

A cross-sectional schematic with the compacted bentonite layer and instrumentation locations is shown in Figure 3(b). The compaction conditions for the soil layer and the locations of the sensors are summarized in Tables 2 and 3, respectively. The MX80 bentonite in as-received conditions was first carefully mixed with water to reach a constant gravimetric water content of 12.55% and stored in a sealed container to ensure homogeneity. Then the bentonite was compacted into eight 25.5 mm-thick lifts with the goal of reaching a target height of 204 mm. However, due to the inclusion of sensors in the bentonite layer during compaction, the final thickness of the layer was 210.5 mm. The heating element was installed after the placement of the second lift in the center of the soil layer, and the third and fourth lifts were compacted around the heating element. The relative humidity sensors were placed atop the fourth lift (at the bottom of the fifth lift), and the dielectric sensors were inserted into the top of the sixth lift so that the sensing probes were within the fifth and sixth lifts. One Type K thermocouple was placed out of the tank to measure room temperature, while the other two were placed at the top of the soil layer above the heating element, and at the inside edge of the container in the middle of the bentonite layer. Two layers of 13 μm-thick plastic wrap were placed on the top of the bentonite layer to help maintain water content before placing the concrete cap. Then, the LVDT was placed on the top of the cap to measure the vertical displacement of the entire soil layer.

Methods and procedures

After the preparation of soil layers and the installation of the sensors, the tank was covered with insulation and the sensors were double-checked. Then, the high-temperature heating process on the compacted bentonite was started with the temperature of the heating element was set to 200 °C to replicate the temperature

expected in the HotBENT project at the Grimsel Test Site (e.g., Zheng et al. 2015; GTS 2022). Time series of the temperatures at the center of the heating element and the ambient room are shown in Figure 4. To better depict the time dependence of temperature over the long duration of the test while still being able to observe the major changes in thermo-hydraulic variables occurring in the early stages of the test this and other time series are plotted on a semilogarithmic scale. All the sensors were scanned every 60 s for the first 24 hours and then every 600 s for the rest of the test.

RESULTS

Time-series results

Evolutions of temperature inside the soil layer from the relative humidity sensors and the dielectric sensors are shown in Figures 5(a) and 5(b), respectively. The results in Figure 5 demonstrated that soil temperatures increase significantly at the first one hundred hours of heating and then close to stable gradually, while the soil temperature close to the heating element always holds a higher temperature than that away from the heating element. Even though the temperature at the center of the heater was 200 °C, due to the low thermal conductivity of the bentonite along with three-dimensional heat transfer effects (e.g., upward and downward heat transfer in addition to radial heat transfer as expected in the repository), the temperature at the location of the nearest sensor (20 mm away) only approached 80 °C. The temperatures for the soils at the top and side boundaries are shown in Figure 6, which indicate that there is appreciable upward heat transfer from the cylindrical heating element, and that the soil at the outer boundary of the container did increase in temperature and stabilize at approximately 28.7 °C, or about 6.1 °C above ambient room temperature.

Although the bentonite in a repository is expected to be restrained both axially and radially, the heating test reported in this study was performed under unconstrained

conditions with a small axial stress of 1.98 kPa. However, the volumetric strains during the heating process were relatively small, as shown in Figure 7. Results show that there is an initial period of negative vertical strain (contraction) at the beginning of heating, while the soil layer started to expand after the temperatures throughout the soil layer increased. The thermal expansion is expected for an over-consolidated soil (e.g., Sultan 2002; Cekerevac and Laloui 2004) or a relatively dry compacted soil under low confinement (e.g., Tang and Cui 2009). Nonetheless, the volumetric strains observed for the soil layer (which had a nonuniform temperature) were smaller than those observed in Tang and Cui (2009). Note that the inflection point in volumetric strain occurs around 100 hours which coincides with the time that the soil temperature stabilizes. Results show that the vertical strain does not increase significantly until the later stages of heating where the soil temperature reaches a high and stable value.

Time series of relative humidity at different locations are shown in Figure 8(a). Results in the figures depicted that the measured relative humidity begins to increase at the beginning of heating, while after several hours of heating, the relative humidity starts to decrease slowly. The initial increase in relative humidity occurs because the water near the heating element was diffused outward during heating, resulting in a temporary wetting front that passes by the sensors. Over time, the wetting front is followed by gradual drying of the bentonite corresponding to a decrease in relative humidity until stabilization. It is important to note that hydraulic stabilization occurs in the soil layer even though the temperature of the bentonite at the center of the layer is close to 200 °C. Although water should completely evaporate from the soil above 100 °C, this likely only occurs in the proximity of the heater. The local degrees of saturation at different locations in the soil layer were calculated from the volumetric water contents measured from the dielectric sensors and the volumetric strain (equal to

the vertical strain) calculated from the LVDT measurements and are plotted in Figure 8(b). Compared with the temperature time series from these sensors in Figure 5(b), the local saturation continues to decrease even after the temperature at this location had stabilized, indicating that the heat transfer and water flow processes occurred at different rates.

Spatial distributions of key variables

Integrating the soil temperature data from different sensors in the middle soil layer, the temperature distributions with radial distances from the heating element are summarized in Figure 9(a). Notably, the soil temperature decreases significantly with radial distance from the heating element for distances less than 125 mm (20 times the heating element radius), the gradient in soil temperature with distance decreases and approaches a stable value. The distributions of the relative humidity and volumetric water content with radial distance from the heating element are summarized in Figures 9(b) and 9(c). Results showed that after thousands of hours of heating, the relative humidity at locations close to the heating element (20, 40 mm) stabilize gradually, and the time required for the relative humidity to stabilize is longer than the time required for the temperature to stabilize, confirming that the times required to reach steady-state distributions in the degree of saturation and temperature may be different depending on the coupling between the thermal and hydraulic properties of a given soil. The overall stability line is approximately in an "S" shape. Moreover, for the locations away from the heating element, the "stable" of water distribution seem would take a much longer time, as the water continues diffusing outward accompanied by the heat transfer from the heating element, while the unsaturated hydraulic conductivity of compacted bentonite is extremely low (e.g., 10^{-12} m/s) (e.g., Pusch 1980; Cui et al. 2008). In fact, it may be difficult for water distribution to reach a stable condition during heating but

may reach a dynamic "thermo-hydraulic equilibrium" stage in a sealed space.

ANALYSIS

Movement of wetting and drying fronts

Significant changes of water distribution in the compacted bentonite occurred during heating. The time series of the degree of saturation in Figure 8(b) indicates that there were three stages of water flow, an initial stage, a wetting stage, and a drying stage. The initial stage corresponds to the initial degree of saturation of the soil layers before heating and at the first few minutes where not enough heat arrived at target locations. The wetting stage occurs at the beginning of heating when the water between the heating element and the sensor disperses outward accompanied by heat transfer, resulting in an outward movement of the wetting front. Thermal-induced flow of water between intra-aggregate pores, where the density of water is greater than that of free water, and inter-aggregate pores containing free water may occur, further increasing the local degree of saturation. However, as heat transfer continues, the water on the inner sides of the sensor reached a thermohydraulic equilibrium gradually and the thermal-induced dispersion at the sensor's location plays a dominant role, resulting in the movement of the drying front. Thus, the degree of saturation decreases corresponds to the drying stage in the figure. The maximum value of the degree of saturation that was observed as the wetting front passed the locations of the different sensors is shown in Figure 10. Notably, the saturation of the wetting front at different locations decreases with the distance from the heating element with an approximately linear function, due to the linearly increasing sectional area. Meanwhile, the velocity of the wetting front, calculated by the distance from the heating element divided by the elapsed time, decreases with distance almost linearly in the semi-logarithmic coordinate system.

Evaluation of the transient SWRC

To understand the transient water retention path of the bentonite during the heating process, the data from the relative humidity sensors and the dielectric sensors were integrated and then transient scanning SWRCs were determined. Kelvin's law was used to convert the relative humidity to total suction, as follows:

$$s_T = -\rho_w \frac{R_g T}{M_w} \ln(RH) \quad (1)$$

where s_T is total suction, ρ_w is the density of water (0.998 Mg/m^3 at 20 ℃), R_g is the universal gas constant (8.31432 J/mol•K), T is the absolute temperature in K, M_w is the relative molar mass of water molecules (18.016 g/mol), and RH is the relative humidity.

The transient SWRCs depict the degree of saturations versus suctions for three locations (50, 60, 100 mm from the heating element) are shown in Figure 11(a). Certain data at specific locations was calculated by the arithmetic mean value of the two adjacent locations. For example, the volumetric water content for point 60 mm (from the heating element) was calculated by the points 50 mm and 70 mm, and then the degree of saturation was calculated correspondingly. Note that each curve in the figure can be divided into two parts based on the turning points, which correspond to a wetting path and drying path, respectively. In another word, the tested curve starts from the wetting path and transitions to a drying path, then follows the drying path. The wetting path, corresponding to the rapid increase of temperature in Figure 11(b), was caused by the water diffusing away from the heater during the initial stage of heating while the drying path corresponds to the gradual drying process in Figure 11(b). It is likely that the initial wetting path follows a scanning curve starting from the primary wetting curve with negligible changes in suction, then follows the primary drying path where larger changes in suction occur as the bentonite dries. The transient path confirms that the

bentonite experiences significant hysteresis during the heating process.

To provide additional context for the transient saturation-suction curves at different locations, the fitted primary wetting and drying paths of the SWRCs fitted by the modified Lu (2016) model were plotted in Figure 11(a) with fitting parameters presented in Table 4. In this model, the water retention due to adsorption and capillary effects are considered separately as follows:

$$S = \frac{\theta(\psi)}{\theta_s} = \frac{\theta_a(\psi) + \theta_c(\psi)}{\theta_s} \quad (2)$$

$$\theta_a(\psi) = \theta_{max}\left\{1 - \left[\exp\left(\frac{\psi - \psi_{max}}{\psi}\right)\right]^m\right\} \quad (3)$$

$$\theta_c(\psi) = \frac{1}{2}\left[1 - \mathrm{erf}\left(\sqrt{2}\frac{\psi - \psi_c}{\psi_c}\right)\right][\theta_s - \theta_a(\psi)]\left[1 + (\alpha\psi)^n\right]^{1/n - 1} \quad (4)$$

where S is degree of saturation (m^3/m^3), $\theta(\psi)$ is the volumetric water content (m^3/m^3), $\theta_a(\psi)$ and $\theta_c(\psi)$ are the adsorptive and capillary volumetric water contents, respectively (m^3/m^3), θ_s is the volumetric water content at saturation or the porosity (m^3/m^3), θ_{max} is the maximum adsorptive volumetric water content (m^3/m^3), ψ is the suction (kPa), ψ_c is the mean cavitation suction (kPa), ψ_{max} is the maximum suction (kPa), α, m, n are fitting parameters, and erf is the error function (e.g., Mathews and Walker 1970).

The wetting path SWRC (Fitted (a)), which is very similar to that fitted to the vapor equilibrium tests shown in Figure 2(b), passes through the initial point of the tested SWRCs, representing the initial hydraulic state for the compacted bentonite. The drying path curve under room temperature (Fitted (b)) shows notable hysteresis with the wetting path curve (Fitted (a)), while the drying path curve (Fitted (c)) shows a shift with elevated temperature. For the wetting path of the SWRCs (Figure 11(a)), the curve for the location closest to the heating element (which has a high temperature as shown in Figure 11(b)) is lower than the curve for the locations further from the heating element with lower temperatures, indicating that the water retention capacity of

bentonite decreases with the increase of temperature at a given suction. This process may occur because the adsorption of water molecules to the surface of the solid phase is an exothermic process, while the desorption of adsorbed water from the surface of the solid phase is an endothermic process. Thus, increased temperature will inhibit the adsorption process of water molecules on the crystal layer surface. In another word, the retention of adsorbed water will be decreased. However, the drying path curve for the location closest to the heating element with the highest temperature, is notably higher than the curve corresponding to locations further from the heating element with lower temperature. This might be due to a change in pore water and pore structure during the transient heat transfer and water flow process. At the beginning of heating, the free water which includes the original free water and newly generated free water diffusing from the locations close to the heater, the curve follows the wetting path. As a result, the soil away from the heating element holds higher water content which will reduce as the soil swells and then compresses the soil closer to the heating element. Therefore, the soil near the heating element will have an increased dry density and more small pores that can retain more water by capillarity. That is the reason why the tested curve following the drying path is higher than the fitted SWRC from the Lu (2016) model, as the increased local dry density causes the SWRC to shift upward.

CONCLUSIONS

This paper presents a tank-scale test setup and experimental methodology to investigate the coupled thermo-hydraulic response of MX80 bentonite during heating. Soil temperature increases notably during the initial stages of heating before gradually stabilizing. A very sharp drop in temperature with distance from the heater was observed. The degree of saturation and relative humidity were found to first increase then decrease as water moved outward away from the central heater. The water flow

process required a longer time to reach equilibrium compared to the heat transfer process. The bentonite experienced a complex wetting and drying path with the movement of the wetting front upon heating. Transient heating causes wetting from the initial primary wetting SWRC path along a scanning curve, after which the bentonite follows the primary drying SWRC path. The bentonite not only shows significant hysteresis between the wetting and drying paths, but also a shift with elevated temperature. The results from this study confirm that it is critical a hysteretic SWRC that incorporates temperature effects when performing numerical simulations of the coupled heat transfer and water flow processes in bentonite buffer systems for nuclear waste repositories, which is worth noting from the current state of the practice.

ACKNOWLEDGEMENTS

The authors appreciate support from US Department of Energy Nuclear Energy University Program award DE-NE008951. The views in this paper are those of the authors alone.

REFERENCES

Åkesson, M., A. C. Jacinto, C. Gatabin, M. Sanchez, and A. Ledesma. 2009. "Bentonite THM behavior at high temperatures: Experimental and numerical analysis." *Géotechnique* 59, no. 4: 307–318. https://doi.org/10.1680/geot.2009.59.4.307

~~Alonso, E. E., J. Alcoverro, F. Coste, L. Malinsky, V. Merrien-Soukatchoff, I. Kadiri, T. Nowak, H. Shao, T. S. Nguyen, A. P. S. Selvadurai, G. Armand, S. R. Sobolik, M. Itamura, C. M. Stone, S. W. Webb, A. Rejeb, M. Tijani, Z. Maouche, A. Kobayashi, H. Kurikami, A. Ito, Y. Sugita, M. Chijimatsu, L. Börgesson, J. Hernelind, J. Rutqvist, C. -F. Tsang, and P. Jussila. 2005. "The FEBEX benchmark test: Case definition and comparison of modelling approaches." *International Journal of Rock Mechanics and Mining Sciences* 42, nos. 5–6: 611–638.~~

~~Bachmann, J., R. Horton, S. A. Grant, and R. R. van der Ploeg. 2002. "Temperature dependence of water retention curves for wettable and water-repellent soils." *Soil Science Society of America Journal* 66, no. 1: 44–52.~~

~~Bag, R. 2011. Coupled thermo-hydro-mechanical-chemical behaviour of MX80 bentonite in geotechnical applications. Ph.D. Thesis, Cardiff University.~~

Başer, T., Y. Dong, A. M. Moradi, N. Lu, K. Smits, S. Ge, D. Tartakovsky, and J. S. McCartney. 2018. "Role of water vapor diffusion and nonequilibrium phase change in geothermal energy storage systems in the vadose zone." *Journal of Geotechnical and Geoenvironmental Engineering* 144, no. 7: 04018038. https://doi.org/10.1061/(ASCE)GT.1943-5606.0001910

Bennett, C. 2014. An experimental study on the hydraulic conductivity of compacted bentonites in geoenvironmental applications. Ph.D. Thesis, Cardiff University.

Birkholzer, J., J. Houseworth, and C. F. Tsang. 2012. "Geologic disposal of high-level radioactive waste: Status, key issues, and trends." *Annual Review of Environment and Resources*, 37: 79–106. https://doi.org/10.1146/annurev-environ-090611-143314

Börgesson, L., A. Fredrikson, and L. E. Johannesson. 1994. "Heat conductivity of buffer materials." Swedish Nuclear Fuel and Waste Management Co. Report Number SKB-TR—94-29. Stockholm. 63 pg.

Börgesson, L., M. Chijimatsu, T. Fujita, T. S. Nguyen, J. Rutqvist, and L. Jing. 2001. "Thermo-hydro-mechanical characterisation of a bentonite-based buffer material by laboratory tests and numerical back analyses." *International Journal of Rock Mechanics and Mining Sciences* 38, no. 1: 95–104. https://doi.org/10.1016/S1365-1609(00)00067-8

Bouyoucos, G. J. 1915. "Effect of temperature on movement of water vapor and

capillary moisture in soils." *Journal of Agricultural Research* 5, no. 4: 141–172. https://handle.nal.usda.gov/10113/IND43965582

Campbell, G. S. 1985. *Soil Physics with Basic, Transport Models for Soil-Plant Systems*. Elsevier, Amsterdam, Netherlands.

Cekerevac, C., and L. Laloui. 2004. "Experimental study of thermal effects on the mechanical behaviour of a clay." *International Journal for Numerical and Analytical Methods in Geomechanics* 28, no. 3: 209–228. https://doi.org/10.1002/nag.332

~~Choi, J. W., and D. W. Oscarson 1996. "Diffusive transport through compacted Na-and Ca-bentonite." *Journal of Contaminant Hydrology* 22, nos. 3–4: 189–202.~~

Cuevas, J., M. V. Villar, A. M. Fernández, P. Gómez, and P. L. Martín. 1997. "Pore waters extracted from compacted bentonite subjected to simultaneous heating and hydration." *Applied Geochemistry* 12, no. 4: 473–481. https://doi.org/10.1016/S0883-2927(97)00024-3

Cui, Y. J., A. M. Tang, C. Loiseau, and P. Delage. 2008. "Determining the unsaturated hydraulic conductivity of a compacted sand-bentonite mixture under constant-volume and free-swell conditions." *Physics and Chemistry of the Earth, Parts A/B/C* 33, no. S1: S462–S471. https://doi.org/10.1016/j.pce.2008.10.017

Cui, Y. J. 2017. "On the hydro-mechanical behaviour of MX80 bentonite-based materials." *Journal of Rock Mechanics and Geotechnical Engineering* 9, no. 3: 565–574. https://doi.org/10.1016/j.jrmge.2016.09.003

De Jonge, L.W., O. H. Jacobsen, and P. Moldrup. 1999. "Soil water repellency: Effects of water content, temperature, and particle size." *Soil Science Society of America Journal* 63, no. 3: 437–442. https://doi.org/10.2136/sssaj1999.03615995006300030003x

de Vries, D. A. 1958. "Simultaneous Transfer of Heat and Moisture in Porous Media." *Eos, Transactions American Geophysical Union* 39, no. 5: 909–916. https://doi.org/10.1029/TR039i005p00909

Dueck, A., and U. Nilsson. 2010. "*Thermo-Hydro-Mechanical Properties of MX-80. Results from Advanced Laboratory Tests*." SKB Technical Report TR-10-55. Lulea, Sweden.

Gawin, D., P. Baggio, and B. A. Schrefler. 1995. "Coupled Heat, Water and Gas Flow in Deformable Porous Media." *International Journal for Numerical Methods in Fluids* 20, nos. 8–9: 969–987. https://doi.org/10.1002/fld.1650200817

Gens, A., A. J. Garcia-Molina, S. Olivella, E. E. Alonso, and F. Huertas. 1998. "Analysis of a full scale in situ test simulating repository conditions." *International Journal for Numerical and Analytical Methods in Geomechanics* 22, no. 7: 515–548. https://doi.org/10.1002/(SICI)1096-9853(199807)22:7<515::AID-NAG926>3.0.CO;2-8

Gens, A., J. Vaunat, B. Garitte, and Y. Wileveau. 2007. "In situ behavior of a stiff layered clay subject to thermal loading: Observations and interpretation." *Géotechnique* 57, no. 2: 207–228. https://doi.org/10.1680/geot.2007.57.2.207

Grimsel Test Site (GTS). 2022. HotBENT Introduction. /web/20220525182521/https://grimsel.com/gts-projects/hotbent-high-temperature-effects-on-bentonite-buffers/hotbent-introduction, Accessed on 05/25/2022.

Gurr, C. G., T. J. Marshall, and J. T. Hutton. 1952. "Movement of water in soil due to a temperature gradient." *Soil Science* 74, no. 5: 335–346.

Henderson-Sellers, B. 1984. "A new formula for latent heat of vaporization of water as a function of temperature." *Quarterly Journal of the Royal Meteorological Society* 110, no. 466: 1186–1190. https://doi.org/10.1002/qj.49711046626

Hoffmann, C., E. E. Alonso, and E. Romero. 2007. "Hydro-mechanical behaviour of bentonite pellet mixtures." *Physics and Chemistry of the Earth, Parts A/B/C* 32, nos. 8–14, 832–849.

Jacinto, A. C., M. V. Villar, R. Gómez-Espina, and A. Ledesma. 2009. "Adaptation of the van Genuchten expression to the effects of temperature and density for compacted bentonites." *Applied Clay Science* 42, no. 3–4: 575–582. https://doi.org/10.1016/j.clay.2008.04.001

Jacinto, A. C., M. V. Villar, and A. Ledesma. 2012. "Influence of water density on the water-retention curve of expansive clays." *Géotechnique* 62, no. 8: 657–667.

Kell, G. S. 1977. "Effects of isotopic composition, temperature, pressure, and dissolved gases on the density of liquid water." *Journal of Physical and Chemical Reference Data* 6, no. 4: 1109–1131. https://doi.org/10.1063/1.555561

Kestin, J., M. Sokolov, and W. A. Wakeham. 1978. "Viscosity of liquid water in the range –8 °C to 150 °C." *Journal of Physical and Chemical Reference Data* 7, no. 3: 941–948. https://doi.org/10.1063/1.555581

Kim, J., W. Hwang, and Y. Kim. 2018. "Effects of hysteresis on hydro-mechanical behavior of unsaturated soil." *Engineering Geology* 245:, 1–9. https://doi.org/10.1016/j.enggeo.2018.08.004

Lee, J. O., H. Choi, and J. Y. Lee. 2016. "Thermal conductivity of compacted bentonite as a buffer material for a high-level radioactive waste repository." *Annals of Nuclear Energy* 94: 848–855. https://doi.org/10.1016/j.anucene.2016.04.053

Lloret, A., and E. E. Alonso. 1985. "State surfaces for partially saturated soils." In *Proceedings of the 11th International Conference on Soil Mechanics and Foundation Engineering*, vol. 2, 557–562. San Francisco, CA.

Lloret, A., M. V. Villar, M. Sánchez, A. Gens, X. Pintado, and E. E. Alonso. 2003.

"Mechanical behaviour of heavily compacted bentonite under high suction changes." *Géotechnique* 53, no. 1: 27–40. https://doi.org/10.1680/geot.2003.53.1.27

Lu, N., and M. Khorshidi. 2015. "Mechanisms for soil-water retention and hysteresis at high suction range." *Journal of Geotechnical and Geoenvironmental Engineering* 141, no. 8: 04015032. https://doi.org/10.1061/(ASCE)GT.1943-5606.0001325

Lu, N. 2016. "Generalized soil water retention equation for adsorption and capillarity." *Journal of Geotechnical and Geoenvironmental Engineering* 142, no. 10: 04016051. https://doi.org/10.1061/(ASCE)GT.1943-5606.0001524

Lu, Y., W. M. Ye, Q. Wang, Y. H. Zhu, Y. G. Chen, and B. Chen. 2020. "Investigation on anisotropic thermal conductivity of compacted GMZ bentonite." *Bulletin of Engineering Geology and the Environment* 79, no. 3: 1153–1162. https://doi.org/10.1007/s10064-019-01636-6

Martín, P. L., and J. M. Barcala. 2005. "Large Scale Buffer Material Test: Mock-Up Experiment at CIEMAT." *Engineering Geology* 81, no. 3: 298–316. https://doi.org/10.1016/j.enggeo.2005.06.013

Mathews, J., and R. L. Walker. 1970. Mathematical Methods of Physics. New York: WA Benjamin.

Moradi, A., K. M. Smits, J. Massey, A. Cihan, and J. McCartney. 2015. "Impact of coupled heat transfer and water flow on soil borehole thermal energy storage (SBTES) systems: Experimental and modeling investigation." *Geothermics* 57: 56–72. https://doi.org/10.1016/j.geothermics.2015.05.007

Philip, J. R., and D. A. de Vries. 1957. "Moisture Movement in Porous Materials under Temperature Gradients." *Eos, Transactions American Geophysical Union* 38, no. 2: 222–232. https://doi.org/10.1029/TR038i002p00222

~~Pintado, X., A. Ledesma, and A. Lloret. 2002. "Back analysis of thermohydraulic bentonite properties from laboratory tests." *Engineering Geology* 64, nos. 2–3: 91–115.~~

Pusch. R. 1979. "Highly compacted sodium bentonite for isolating rock-deposited radioactive waste products." *Nuclear Technology* 45, no. 2: 153–157. https://doi.org/10.13182/NT79-A32305

Pusch, R. 1980. *Permeability of highly compacted bentonite*. Swedish Nuclear Fuel and Waste Management Company. Technical Report 80-16.

~~Pusch, R. 1992. "Use of bentonite for isolation of radioactive waste products." *Clay Minerals* 27, no. 3: 353–361.~~

Rawat, A., W. Baille, and S. Tripathy. 2019. "Swelling behavior of compacted bentonite-sand mixture during water infiltration." *Engineering Geology* 257 ~~(July)~~: 105141. https://doi.org/10.1016/j.enggeo.2019.05.018

Rawat, A., L. Lang, W. Baille, A. C. Dieudonne, and F. Collin. 2020. "Coupled hydro-mechanical analysis of expansive soils: Parametric identification and calibration." *Journal of Rock Mechanics and Geotechnical Engineering* 12, no. 3: 620–629. https://doi.org/10.1016/j.jrmge.2019.12.013

Rawat, A., W. Baille, S. Tripathy, and T. Schanz. 2021. "A column-type experimental device for investigating coupled thermo-hydro-mechanical behavior of expansive soils." *Geotechnical Testing Journal* 44, no. 6: 1559–1576. https://doi.org/10.1520/GTJ20180192

Revil, A., and N. Lu. 2013. "Unified water sorption and desorption isotherms for clayey porous materials." *Water Resources Research* 49, no. 9: 5685–5699. https://doi.org/10.1002/wrcr.20426

Romero, E., A. Gens, and A. Lloret. 2001. "Temperature effects on the hydraulic

behaviour of an unsaturated clay." In: Toll, D.G. (eds) *Unsaturated Soil Concepts and Their Application in Geotechnical Practice*. Springer, Dordrecht. https://doi.org/10.1007/978-94-015-9775-3_5

Romero, E., A. Gens, and A. Lloret. 2003. "Suction effects on a compacted clay under non-isothermal conditions." *Géotechnique* 53, no. 1: 65–81. https://doi.org/10.1680/geot.2003.53.1.65

Romero, E., G. Della Vecchia, and C. Jommi. 2011. "An insight into the water retention properties of compacted clayey soils." *Géotechnique* 61, no. 4: 313–328. https://doi.org/10.1680/geot.2011.61.4.313

Rostami, A., G. Habibagahi, M. Ajdari, and E. Nikooee. 2015. "Pore network investigation on hysteresis phenomena and influence of stress state on the SWRC." *International Journal of Geomechanics* 15, no. 5: 04014072. https://doi.org/10.1061/(ASCE)GM.1943-5622.0000315

Saba, S., J. D. Barnichon, Y. J. Cui, A. M. Tang, and P. Delage. 2014a. "Microstructure and anisotropic swelling behaviour of compacted bentonite/sand mixture." *Journal of Rock Mechanics and Geotechnical Engineering* 6, no. 2: 126–132. https://doi.org/10.1016/j.jrmge.2014.01.006

Saba, S., Y. J. Cui, A. M. Tang, and J. D. Barnichon. 2014b. "Investigation of the swelling behaviour of compacted bentonite-sand mixture by mock-up tests." *Canadian Geotechnical Journal* 51, no. 12: 1399–1412. https://doi.org/10.1139/cgj-2013-0377

Sánchez, M., A. Gens, L. do Nascimento Guimarães, and S. Olivella. 2005. "A double structure generalized plasticity model for expansive materials." *International Journal for Numerical and Analytical Methods in Geomechanics* 29, no. 8: 751–787. https://doi.org/10.1002/nag.434

~~Sawatsky, N. G., and D. W. Oscarson. 1991. "Diffusion of technetium in dense bentonite." *Water, Air, and Soil Pollution* 57, no. 1 449–456.~~

Schanz, T., L. Nguyen-Tuan, and M. Datcheva. 2013. "A column experiment to study the thermo-hydro-mechanical behavior of expansive soils." *Rock Mechanics and Rock Eng.* 46, no. 6: 1287–1301. https://doi.org/10.1007/s00603-012-0361-8

~~Smits, K. M., A. Cihan, S. Sakaki, and T. H. Illangasekare. 2011. "Evaporation from soils under thermal boundary conditions: Experimental and modeling investigation to compare equilibrium- and nonequilibrium based approaches." *Water Resources Research* 47, no. 5 (May): W05540.~~

Sultan, N., P. Delage, and Y. J. Cui. 2002. "Temperature effects on the volume change behaviour of Boom clay." *Engineering Geology* 64, nos. 2–3: 135–145. https://doi.org/10.1016/S0013-7952(01)00143-0

Tang, A. M., and Y. J. Cui. 2005. "Controlling suction by vapour equilibrium technique at different temperatures, application to the determination of the water retention properties of MX80 clay." *Canadian Geotechnical Journal* 42, no. 1: 287–296. https://doi.org/10.1139/t04-082

Tang, A. M., and Y. J. Cui. 2009. "Modelling the thermomechanical volume change behaviour of compacted expansive clays." *Géotechnique* 59, no. 3: 185–195. https://doi.org/10.1680/geot.2009.59.3.185

Thomas, H. R., and S. D. King. 1991. "Coupled temperature capillary potential variations in unsaturated soil." *Journal of Engineering Mechanics* 117, no. 11: 2475–2491. https://doi.org/10.1061/(ASCE)0733-9399(1991)117:11(2475)

~~Thomas, H. R., Y. He, M. R. Sansom, and C. L. W. Li. 1996. "On the development of a model of the thermo-mechanical-hydraulic behavior of unsaturated soils." *Engineering Geology* 41, nos. 1–4: 197–218.~~

Thomas, H. R., and Y. He. 1997. "A coupled heat-moisture transfer theory for deformable unsaturated soil and its algorithmic implementation." *International Journal for Numerical Methods in Engineering* 40, no. 18: 3421–3441. https://doi.org/10.1002/(SICI)1097-0207(19970930)40:18<3421::AID-NME220>3.0.CO;2-C

Tripathy, S., R. Bag, and H. R. Thomas. 2014. "Effects of post-compaction residual lateral stress and electrolyte concentration on swelling pressures of a compacted bentonite." *Geotechnical and Geological Engineering* 32, no. 4: 749–763. https://doi.org/10.1007/s10706-014-9754-7

Tripathy, S., H. R. Thomas, and R. Bag. 2015. "Geoenvironmental application of bentonites in underground disposal of nuclear waste: Characterization and Laboratory Tests." *Journal of Hazardous, Toxic, and Radioactive Waste* 21, no. 1: 1–12. https://doi.org/10.1061/(ASCE)HZ.2153-5515.0000272

Tripathy, S., H. R. Thomas, and P. Stratos. 2017. "Response of compacted bentonites to thermal and thermo-hydraulic loadings at high temperatures." *Geosciences* 7, no. 3: 53. https://doi.org/10.3390/geosciences7030053

Tuller, M., D. Or, and L. M. Dudley. 1999. "Adsorption and capillary condensation in porous media: Liquid retention and interfacial configurations in angular pores." *Water Resources Research* 35, no. 7: 1949–1964. https://doi.org/10.1029/1999WR900098

Villar, M.V., and A. Lloret, A. 2004. "Influence of temperature on the hydro-mechanical behaviour of a compacted bentonite." *Applied Clay Science* 26, no. 1: 337–350. https://doi.org/10.1016/j.clay.2003.12.026

Villar, M. V. 2005. MX-80 Bentonite. Thermal-Hydro-Mechanical characterisation performed at CIEMAT in the context of the prototype project. CIEMAT-1053.

Spain.

~~Villar, M. V., P. L. Martín, and J. M. Barcala. 2005. "Modification of physical, mechanical and hydraulic properties of bentonite by thermo-hydraulic gradients." *Engineering Geology* 81, no. 3: 284–297.~~

Villar, M. V., R. J. Iglesias, J. L. García-Siñeriz, A. Lloret, and F. Huertas. 2020. "Physical evolution of a bentonite buffer during 18 years of heating and hydration." *Engineering Geology* 264: 105408. 10.1016/j.enggeo.2019.105408

Wang, Q., A. M. Tang, Y. J. Cui, P. Delage, and B. Gatmiri. 2012. "Experimental study on the swelling behaviour of bentonite/claystone mixture." *Engineering Geology* 124: 59–66. https://doi.org/10.1016/j.enggeo.2011.10.003

Xu, L., W. M. Ye, and B. Ye. 2017. "Gas breakthrough in saturated compacted GaoMiaoZi (GMZ) bentonite under rigid boundary conditions." *Canadian Geotechnical Journal* 54, no. 8: 1139–1149. https://doi.org/10.1139/cgj-2016-0220

Ye, W. M., Y. J. Cui, L. X. Qian, and B. Chen. 2009. "An experimental study of the water transfer through confined compacted GMZ bentonite." *Engineering Geology* 108, nos. 3–4: 169–176. https://doi.org/10.1016/j.enggeo.2009.08.003

Ye, W. M., J. Y. Zhu, B. Chen, Y. G. Chen, and Y. J. Cui. 2015. "Experimental investigation on soil-water retention properties of compacted GMZ01 bentonite with consideration of temperature and initial dry density." In *Proceeding of the 10th Asian Regional Conference of IAEG*. Kyoto.

Yong, R. N., A. M. O. Mohamed, I. Shooshpasha, and C. Onofrei. 1997. "Hydro-thermal performance of unsaturated bentonite-sand buffer material." *Engineering Geology* 47, no. 4: 351–365. https://doi.org/10.1016/S0013-7952(96)00115-9

Zheng, L., J. Rutqvist, J. T. Birkholzer, and H. H. Liu. 2015. "On the impact of temperatures up to 200 °C in clay repositories with bentonite engineer barrier

systems: A study with coupled thermal, hydrological, chemical, and mechanical modeling." *Engineering Geology* 197: 278–295. http://doi.org/10.1016/j.enggeo.2015.08.026

Zheng, L., J. Rutqvist, H. Xu, and J. T. Birkholzer. 2017. "Coupled THMC models for bentonite in an argillite repository for nuclear waste: Illitization and its effect on swelling stress under high temperature." *Engineering Geology* 230: 118–129. https://doi.org/10.1016/j.enggeo.2017.10.002

Table 1. Basic physical properties of MX80 bentonite

Parameter	Value
Specific gravity, G_s (%)	2.66
Liquid limit, ω_L (%)	345
Plastic limit, ω_P (%)	47
Plastic index, I_P (-)	298

Table 2. Initial conditions of the soil layer after compaction

Parameter	Value
Thickness (mm)	210.5
Total density (Mg/m^3)	1.472
Dry density (Mg/m^3)	1.308
Gravimetric water content (%)	12.55
Volumetric water content (m^3/m^3)	0.191
Void ratio (m^3/m^3)	1.034
Porosity (m^3/m^3)	0.508
Degree of saturation (m^3/m^3)	0.323

Table 3. Sensor locations

Sensor	No.	Radial distance from heating element surface (mm)	Height from tank bottom (mm)
Heating element	-	-	103
Relative humidity sensors	A	20	103
	B	40	103
	C	60	103
	D	100	103
Dielectric sensors	A	50	103
	B	70	103
	C	100	103
	D	125	103
	E	185	103
Thermocouples (Type K)	A	-	-
	B	0	210.5
	C	277.3	103
External LVDT	-	-	400

765 **Table 4.** Model parameters for the SWRC of Lu (2016)

Parameter	Figure 2(b)	Figure 11(a)		
		Fitted (a)	Fitted (b)	Fitted (c)
θ_s (m^3/m^3)	0.529	0.526	0.526	0.526
θ_{max} (m^3/m^3)	0.219	0.221	0.221	0.230
ψ_c (kPa)	32000	32000	84000	82000
ψ_{max} (kPa)	577750	577750	577750	483450
α (-)	0.05	0.002	0.001	0.0012
m (-)	0.35	0.35	0.99	0.99
n (-)	1.60	1.6	1.5	1.5

766

767

768

List of Figure Captions

Figure 1. Summary of coupled heat transfer and water flow processes in a bentonite buffer

Figure 2. Geotechnical properties of MX80 bentonite: (a) Grain size distribution (b) SWRC

Figure 3. Overview of the tank test setup: (a) Photo of the assembled experimental setup; (b) Schematic with the compacted bentonite layer and instrumentation locations

Figure 4. Central heating element and ambient room temperature boundary conditions

Figure 5. Evolution of soil temperatures inside the bentonite layer obtained from: (a) Relative humidity sensors; (b) Dielectric sensors

Figure 6. Evolution of temperatures at the top-center and side of the soil layer

Figure 7. Evolution of vertical strain during heating (positive strain denotes expansion)

Figure 8. Time series of hydraulic response of the soil layer at different locations during heating: (a) Relative humidity; (b) Degree of saturation

Figure 9. Radial profile plots of thermo-hydraulic variables at different times during heating: (a) Temperature; (a) Relative humidity; (b) Degree of saturation

Figure 10. Saturation at wetting front and velocity of wetting front

Figure 11. Transient thermo-hydraulic response at different locations in the soil layer: (a) Suction-saturation curves with wetting and drying path SWRCs; (b) Temperature-saturation curves

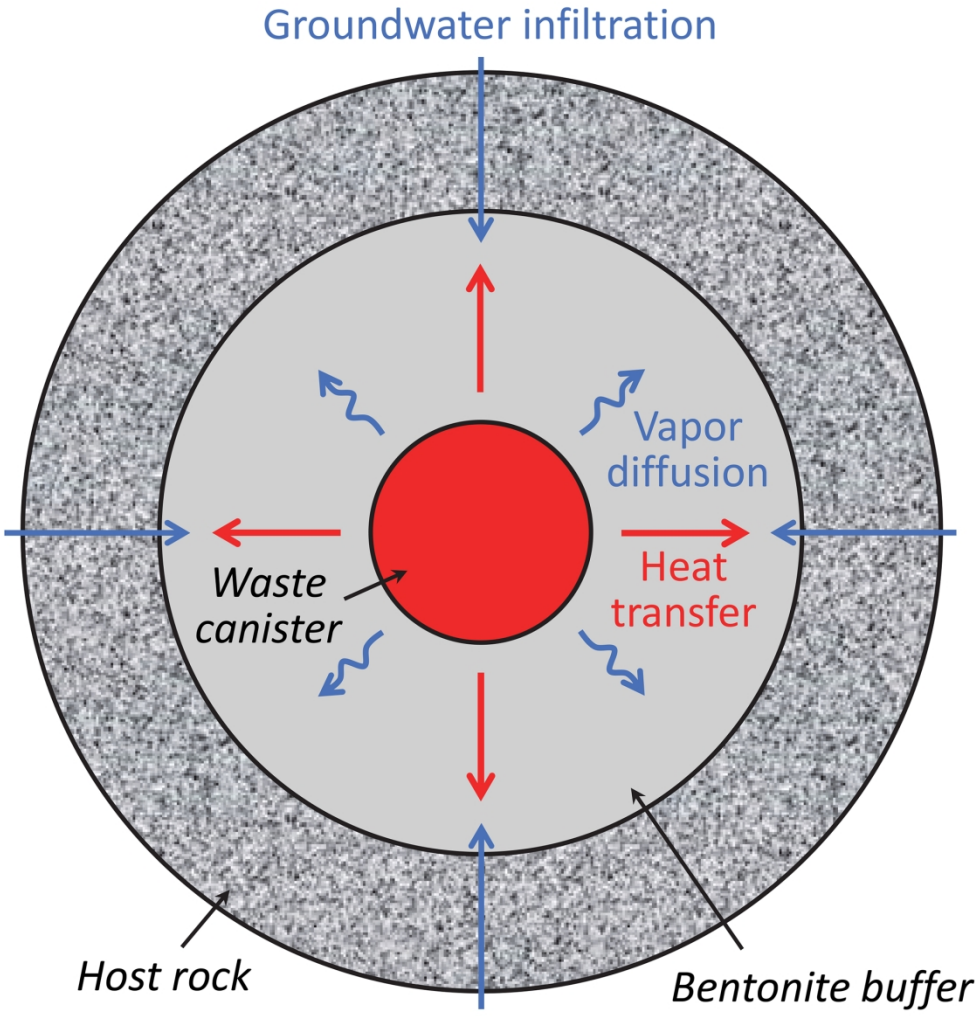

Figure 1. Summary of coupled heat transfer and water flow processes in a bentonite buffer

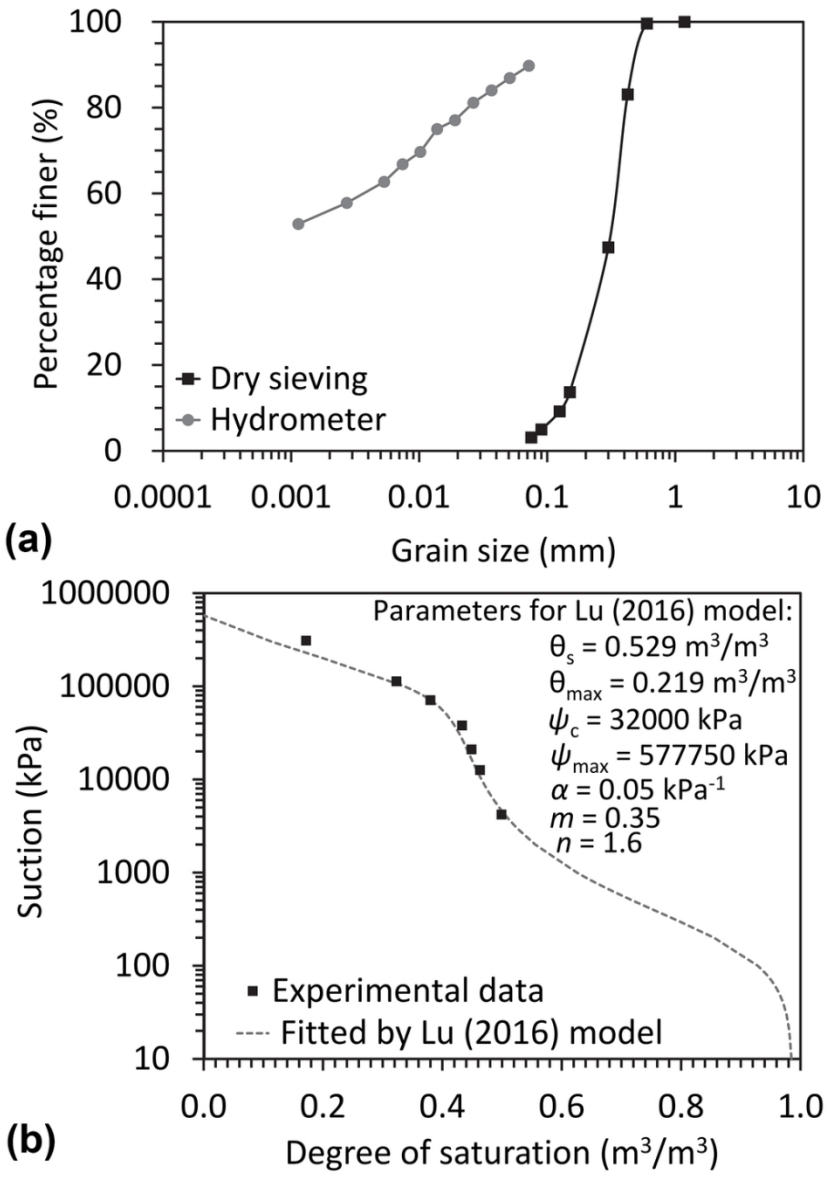

Figure 2. Geotechnical properties of MX80 bentonite: (a) Grain size distribution (b) SWRC

88x126mm (300 x 300 DPI)

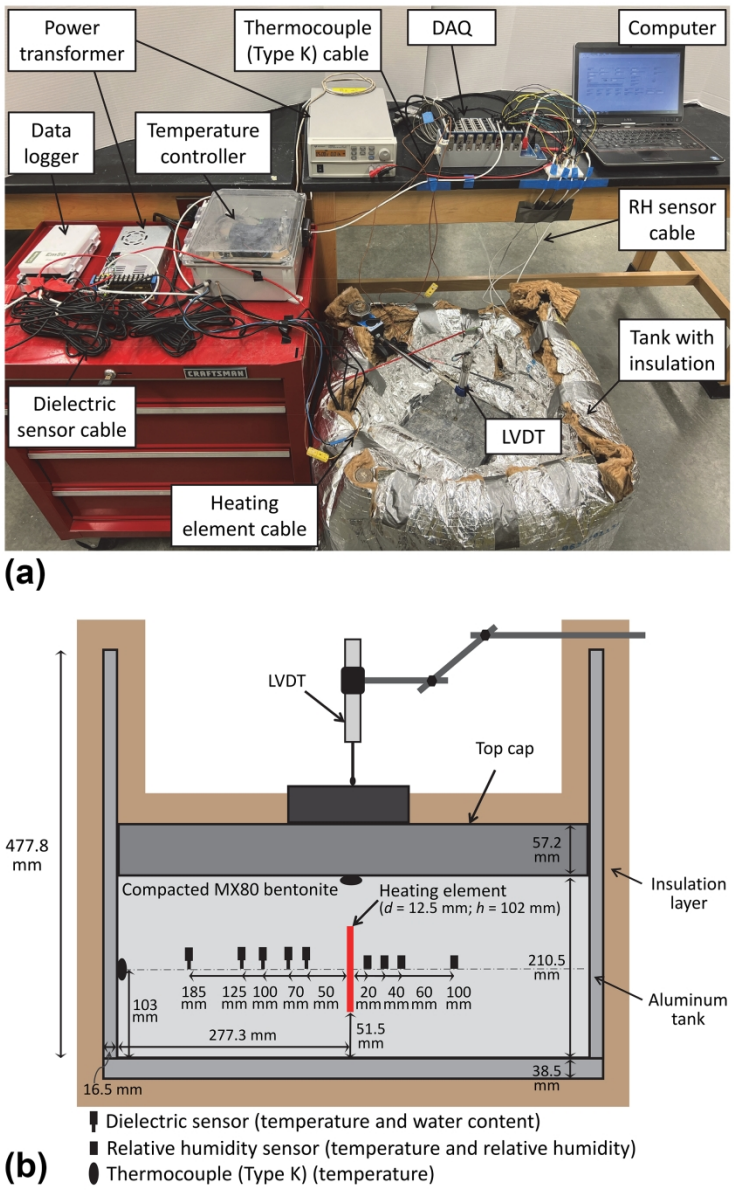

Figure 3. Overview of the tank test setup: (a) Photo of the assembled experimental setup; (b) Schematic with the compacted bentonite layer and instrumentation locations

88x145mm (600 x 600 DPI)

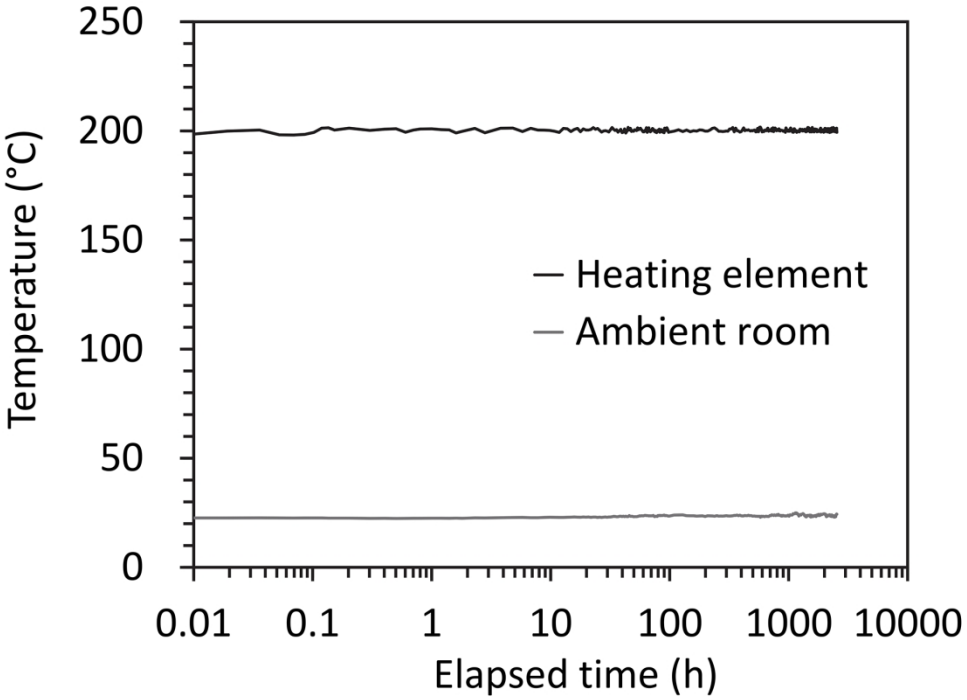

Figure 4. Central heating element and ambient room temperature boundary conditions

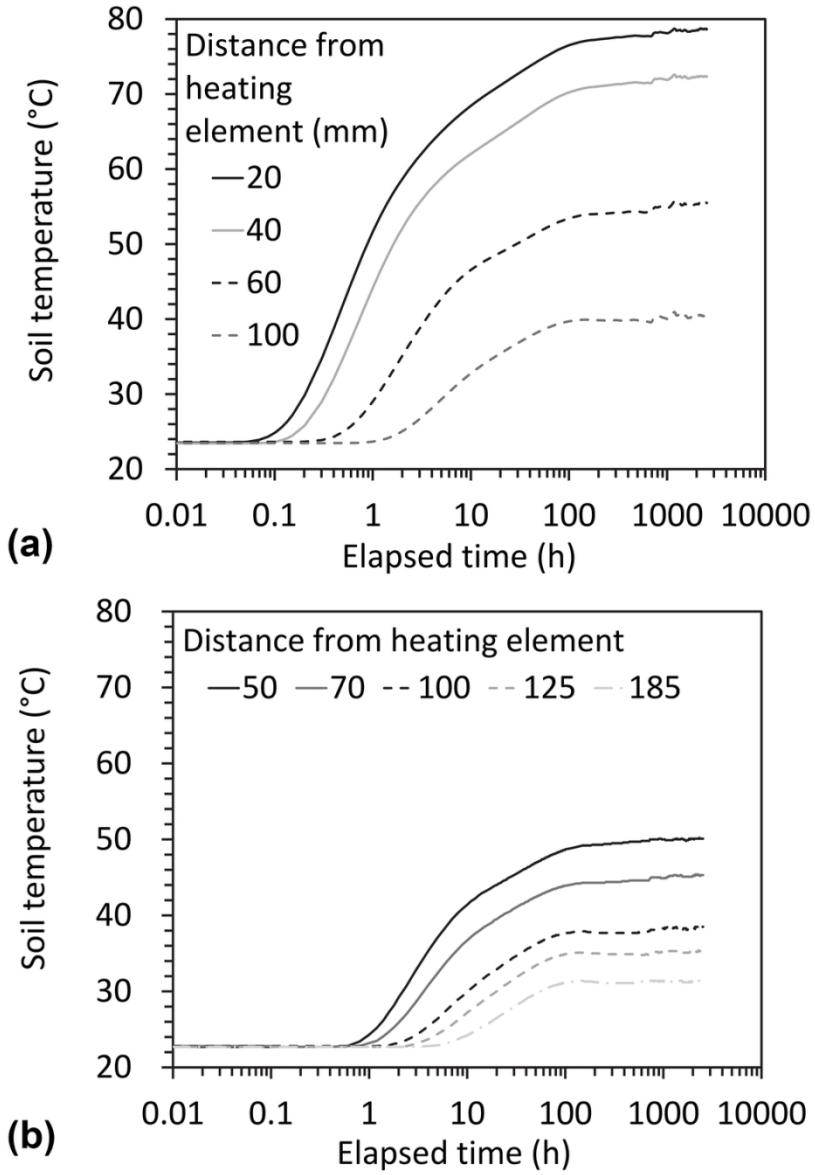

Figure 5. Evolution of soil temperatures inside the bentonite layer obtained from: (a) Relative humidity sensors; (b) Dielectric sensors

88x130mm (300 x 300 DPI)

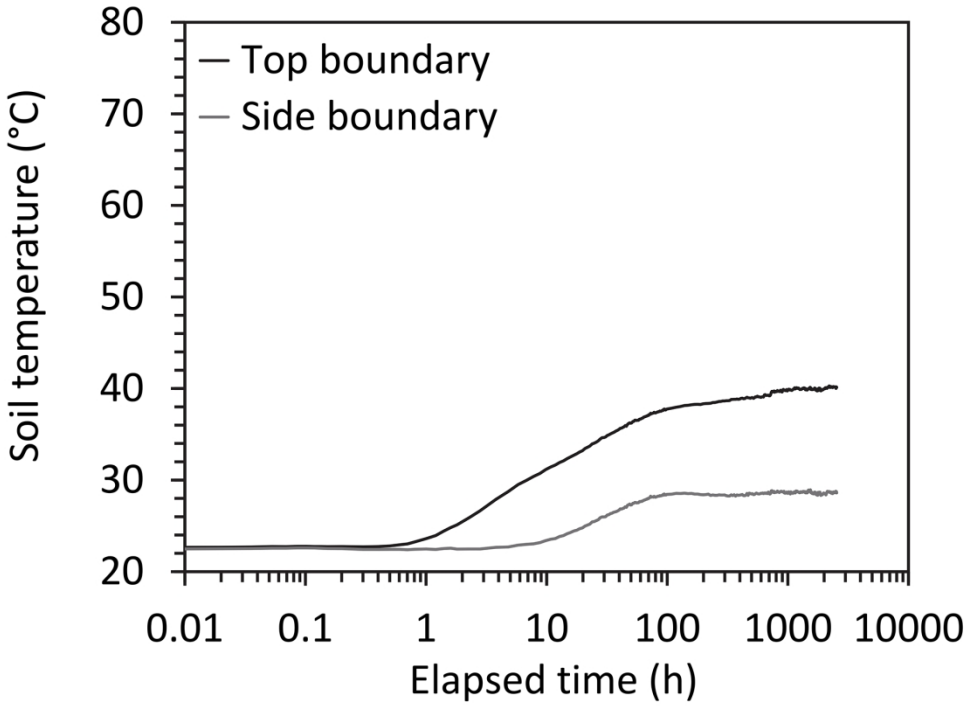

Figure 6. Evolution of temperatures at the top-center and side of the soil layer

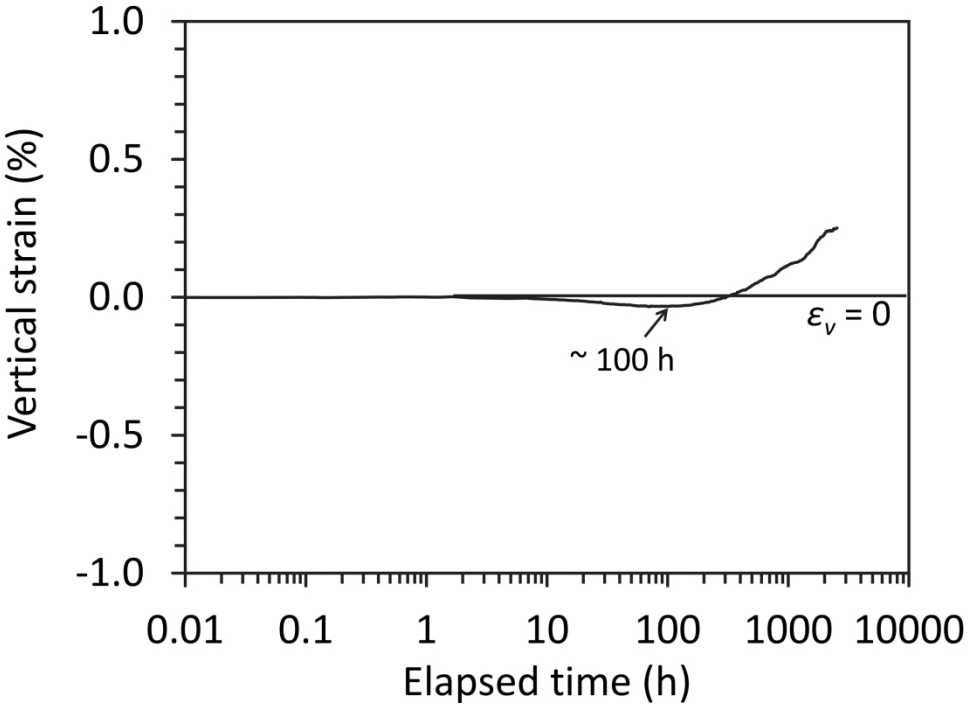

Figure 7. Evolution of vertical strain during heating (positive strain denotes expansion)

240x174mm (300 x 300 DPI)

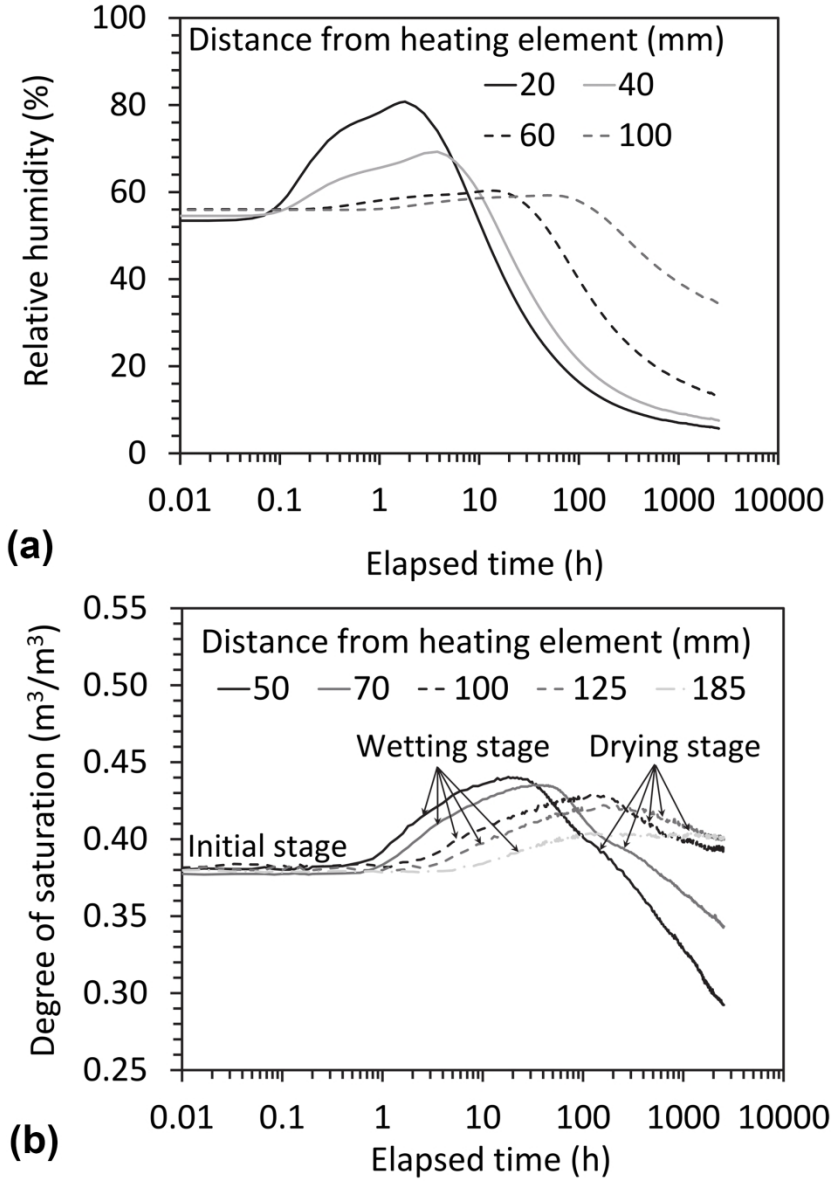

Figure 8. Time series of hydraulic response of the soil layer at different locations during heating: (a) Relative humidity; (b) Degree of saturation

88x128mm (600 x 600 DPI)

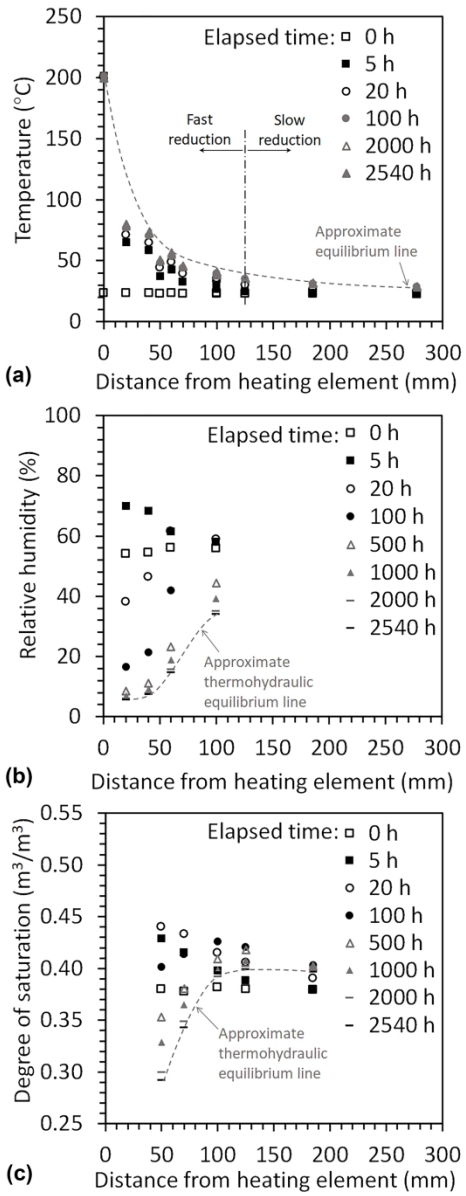

Figure 9. Radial profile plots of thermo-hydraulic variables at different times during heating: (a) Temperature; (a) Relative humidity; (b) Degree of saturation

88x230mm (600 x 600 DPI)

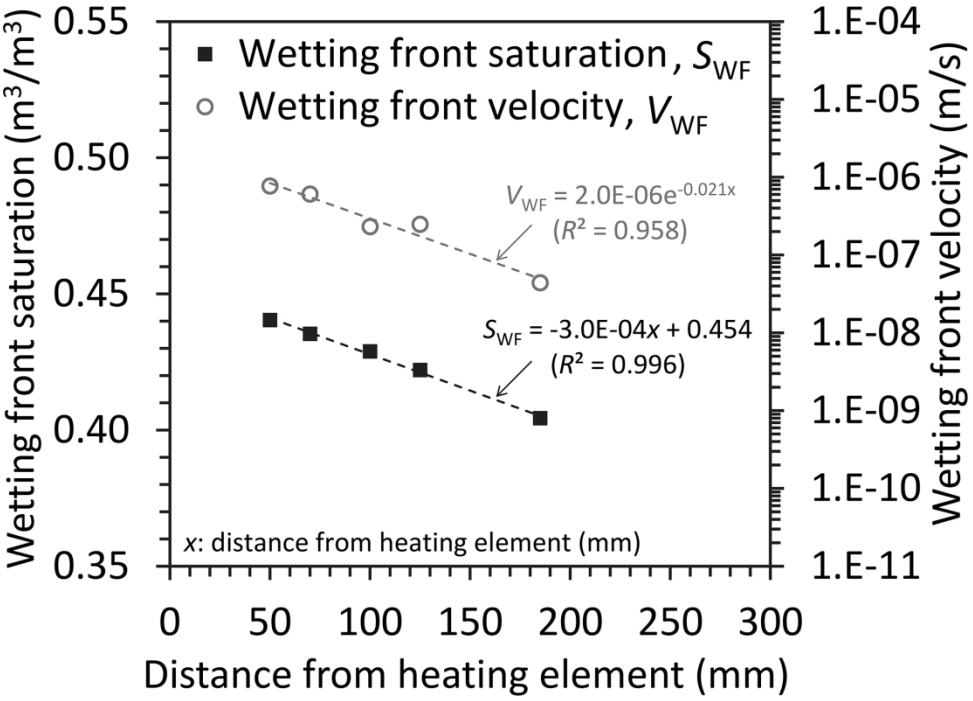

Figure 10. Saturation at wetting front and velocity of wetting front

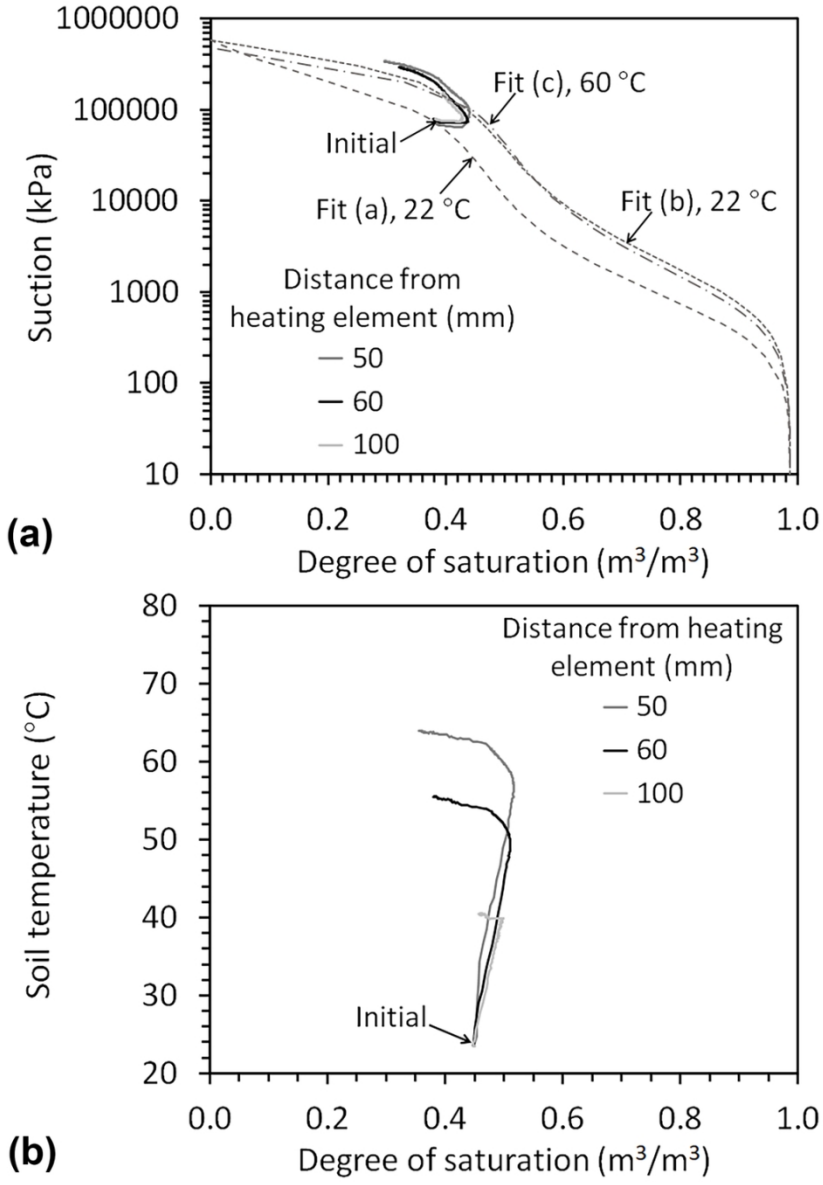

Figure 11. Transient thermo-hydraulic response at different locations in the soil layer: (a) Suction-saturation curves with wetting and drying path SWRCs; (b) Temperature-saturation curves

88x129mm (300 x 300 DPI)